DOI 10.1007/s11085-013-9417-8

Cyclic Oxidation Behavior of TBC Systems with a Pt-Rich γ-Ni+γ′-Ni_3Al Bond-Coating Made by SPS

Pauline Audigié · Serge Selezneff · Aurélie Rouaix-Vande Put · Claude Estournès · Sarah Hamadi · Daniel Monceau

Abstract To obtain long-lasting thermal barrier coating (TBC) systems, two types of Pt-rich γ-Ni+γ′-Ni_3Al bond-coatings (BC) were fabricated by spark plasma sintering (SPS). The former had the highest possible Pt content (Ni-30Pt-25Al in at.%) while the latter had the highest possible Al level (Ni-28Al-17Pt in at.%). Hf was added as a reactive element. TBCs were fabricated on different superalloys (AM1, René N5 and MCNG) with the aforementioned BCs and with zirconia stabilized with yttria top coats made by SPS or electron beam physical vapor deposition (EBPVD). The cyclic oxidation resistance of these systems was studied at 1,100 °C in air. Most TBCs with a Pt-rich γ–γ′ BC showed better thermal cycling resistance when compared to the reference TBCs (β-(Ni,Pt)Al diffusion BC and EBPVD ceramic top coat), with lifetimes up to 1,745 cycles instead of 700 for the

P. Audigié · A. Rouaix-Vande Put · D. Monceau
CIRIMAT, CNRS, ENSIACET, 4 Allée Emile Monso,
BP 44362, 31030 Toulouse, France
e-mail: daniel.monceau@ensiacet.fr

P. Audigié
e-mail: pauline.audigie@ensiacet.fr

A. Rouaix-Vande Put
e-mail: aurelie.rouaix@ensiacet.fr

S. Selezneff
SNECMA, Site de Villaroche, Rond-Point René Ravaud, 77550 Moissy-Cramayel, France
e-mail: serge.selezneff@snecma.fr

C. Estournès
CIRIMAT, CNRS, Université Paul Sabatier, 118 Route de Narbonne, 31062 Toulouse Cedex 9, France
e-mail: estournes@chimie.ups-tlse.fr

S. Hamadi
SNECMA, Site Evry-Corbeil, rue Henri-Auguste Desbruères, 91003 Evry Cedex, France
e-mail: sarah.hamadi@snecma.fr

reference, and despite the fabrication defects observed within the SPS BCs. Cu was tested as an addition in the BCs and proved to have a slight negative effect on the system lifetime. Moreover, the fourth generation MCNG substrate led to the best cyclic oxidation behavior.

Keywords TBC systems · Pt-rich γ-Ni+γ′-Ni_3Al · Bond-coatings · Thermal cycling · Spallation

Introduction

Thermal barrier coating (TBC) systems have been developed in order to protect Ni-base superalloys against excessive oxidation. They are commonly used for blades and vanes in gas turbine engines. TBC systems are multi-layer coating systems composed of a substrate (the superalloy), an Al-rich bond-coating (BC), a thermally grown oxide (TGO) and a top coat made of yttria partially stabilized zirconia (YPSZ). The insulating top coat (or TBC) allows lowering the temperature of the underlying metal. It is usually deposited by electron beam physical vapor deposition (EBPVD) or by atmospheric plasma spraying. The oxidation of the BC leads to the formation and growth of a protective oxide scale, the TGO which is composed mainly of α-alumina, this oxide being an excellent diffusion barrier for oxygen and metal ions.

Recently, a new class of BCs with a γ-Ni+γ′-Ni_3Al microstructure enriched in Pt have been studied in order to improve the TBC system lifetime. These BCs have some advantages over β-(Ni,Pt)Al coatings. In that, no topologically closed packed (TCP) phases form in the interdiffusion zone between the coating and the substrate [1]. The secondary reaction zone is also suppressed between the coating and the substrate when the latter is a fourth-generation superalloy [2]. No detrimental phase transformation takes place as the coating and the substrate have the same crystallographic structure [3]. After thermal cycling, very little or no rumpling is present [4, 5]. It is now well known that Pt-rich γ–γ′ BCs have a better oxidation behavior compared with β-(Ni,Pt)Al coatings [6–8]. However, some issues related to Pt-rich γ–γ′ BCs concern the limited Al reservoir which could prevent alumina formation over long periods [5] and the sensitivity to substrate composition [7–10].

Initially developed to sinter metallic or ceramic powders, spark plasma sintering (SPS) was recently used to fabricate complete TBC systems in a single step [11, 12]. Selezneff [13] had used fast processing with SPS to develop two compositions to get long-lasting Pt-rich γ-Ni+γ′-Ni_3Al BCs. The first and second compositions contained respectively the highest possible level of Pt and Al in the γ′ phase, based on the Ni–Pt–Al phase diagram at 1,100 °C of Hayashi et al. [14]. This work was continued by carrying out a thermal cycling test at 1,100 °C on TBC systems with those previously developed BCs. The effects of the Pt-rich γ-Ni+γ′-Ni_3Al coating composition and of the superalloy composition were studied using TBC systems fully fabricated by SPS. TBC systems containing a BC made by SPS and a top coat deposited by EBPVD were also subjected to thermal cycling to compare the new BCs with the standard system. Cu addition was studied in Selezneff's work [13]

to evaluate its ability to increase the Al content in the γ′ phase [15] to raise the Al reservoir in the coating. It was shown that Cu addition was inefficient to increase Al content in the γ′ phase of a coating [13]. However, the Cu layer addition at the surface of the superalloy appeared to favor the Ni and Pt interdiffusion during the heat treatment in SPS processing leading to a homogeneous γ–γ′ microstructure [13, 16]. Therefore, Cu was added in some γ–γ′ coatings of this study. Spalling was monitored and cross sections were prepared to identify the degradation mechanisms.

Experimental Procedures

TBC System Fabrication

The substrates were 24 mm diameter discs, cut from two cast rods of single crystal first generation Ni-base superalloy AM1, with a low S content (<0.4 wt ppm). The superalloy composition is given in Table 1. The concentration of trace elements was determined by glow discharge mass spectroscopy analysis and is reported in Table 2. A thin layer of the reactive element Hf, with or without an additional Cu layer, was deposited on the substrate before BC manufacturing. The Hf and Cu films were respectively 100 and 200 nm thick and were deposited by radio-frequency-sputtering with a Leybold–Heraus sputtering machine, at ICMCB (Bordeaux, France). The Cu content was estimated by comparing with similar TBC systems containing initially a 900 nm thick Cu film which corresponded to 4 at.% as measured by EPMA. Assuming an uniform Cu repartition in the BC, a 200 nm thick film leads to a concentration of about 1 at.%. To limit their oxidation, samples were kept in Ar before SPS.

Two objectives of BC chemical compositions were investigated: Ni-30Pt-25Al and Ni-28Al-17Pt in at.%. The BCs were fabricated by SPS from a stack of Pt and Al foils. With the SPS process, coating composition is well controlled by Pt and Al foil thicknesses and by heat treatment [11]. The Ni-30Pt-25Al composition was obtained by the addition of a 5 μm thick Pt foil and a 2 μm thick Al foil, hence referred to as the 5/2 composition. The Ni-28Al-17Pt composition was obtained by a stack of Pt and Al foils, 5 μm thick each, hence referred to as the 5/5 composition. After SPS, in order to obtain the γ–γ′ BC microstructure, heat treatments were conducted at 1,100 °C in air. For systems with top coats made by SPS, heat treatments lasted 5 and 25 h, respectively for the 5/2 and 5/5 BCs. For EBPVD top coat, samples were heat treated for 10 h at 1,100 °C and 80 h at 1,000 °C (due to an

Table 1 Superalloy composition (at.%)

Superalloy	Cr	Co	Mo	W	Ta	Re	Ru	Al	Ti	Hf	Ni
AM1 first rod	8.7	6.7	1.3	1.9	2.7	–	–	11.8	1.5	0.02	Bal.
AM1 second rod	9.1	6.7	1.3	1.9	2.6	–	–	11.6	1.4	0.02	
René N5	8.1	8.2	1.3	1.6	2.3	1.0	–	13.9	–	0.07	
MCNG	4.7	–	0.6	1.7	1.7	1.3	2.4	13.6	0.6	0.03	

Table 2 Trace elements in AM1® superalloy (ppma)

Superalloy	Hf	Zr	S	Si	C	N	O
AM1 first rod	173	3	<0.8	121	~245	~2	~12
AM1 second rod	184	4	<0.8	137	~307	~3	~15

experimental issue), corresponding in terms of equivalent Pt diffusion to ~25 h at 1,100 °C.

The SPS apparatus used to fabricate the samples was a Dr Sinter 2080 (SPS Sumitomo Coal Mining Co., Japan). This device enabled to heat the samples using a high intensity current and a low voltage. The current was applied by pulses following the standard 12/2 on/off 3.3 ms pulse pattern. Graphite punches and die were used. A K-type thermocouple placed in a 3 mm-deep hole at the die surface was used to monitor the temperature. This SPS procedure was detailed in [11].

The last layer of the TBCs was the top coat which consisted of an YPSZ deposited either by SPS or EBPVD. In the first case, the BC and the thermal barrier were fabricated in one step during the same SPS cycle. A powder from Tosoh Corporation was used for the YPSZ coating which contained 3 mol% Y_2O_3 i.e. $(ZrO_2)_{0.97}(Y_2O_3)_{0.03}$. In the second case, after SPS BC manufacturing, a light grit-blasting with α-Al_2O_3 particles was performed to clean the BC surface and then the 150 μm thick top coat was deposited by EBPVD at the Ceramic Coating Center at Châtellerault (France).

For comparison purposes, conventional TBC systems composed of a low sulphur AM1 superalloy, a β-(Ni,Pt)Al BC and an EBPVD top coat were also manufactured. A 7 μm thick Pt layer was deposited on the superalloy by electroplating and then a diffusion treatment under vacuum was carried out for 1 h at 1,100 °C. The Al enrichment was done by a vapor phase aluminizing (APVS) process. These reference samples were provided by Snecma (France).

To study the substrate effect, two TBC systems were based on René N5, a second generation superalloy containing Re and no Ti, and on MCNG, a fourth generation superalloy containing Re and Ru. Their nominal compositions are given in Table 1. Hf and Cu layers were deposited on the superalloy surface followed by the 5/2 BC. The 150 μm thick thermal barrier was made using SPS, according to the fabrication process previously described.

Thermal Cycling and Characterization

All TBCs were tested under high temperature cyclic oxidation in air. A cycle was composed of a 1 h dwell at 1,100 °C including a rapid heating followed by a cooling period of 15 min to room temperature. A high cooling rate was obtained using a high flow of air, free from oil and pollution. Pictures of all the samples were taken at different durations during thermal cycling to follow spallation kinetics. Image analyzes enable the assessment of the unspalled area fraction. Some TBCs made by the one-step SPS process were not coated over the entire surface because of defects present close to the sample sides. When this occurred, the actual TBC

surface area at 0 cycle was taken as the reference for the calculation of the fraction of unspalled area. Arbitrarily, the TBC system end of life was considered reached when the TBC spalled surface represented more than 25 % of the entire surface of the sample. Cycling was pursued until the TBC spalled area fraction attained at least 60 %.

In order to understand which mechanism led to the TBC delamination, cross-sections of the samples were observed by scanning electron microscopy (SEM) and analyzed by energy dispersive spectroscopy (EDS) using a LEO 435VP SEM equipped with an IMIX EDS system. The quantification of EDS analyzes was obtained from real standards. Samples denomination of all TBC systems are summed up in Table 3.

Results and Discussion

SPS Systems After Fabrication

SEM observations were performed on all samples after SPS processing and heat treatment at 1,100 °C. Figure 1 shows "one-step" SPS TBC systems with AM1 superalloy exhibiting a microstructure typical of Pt-rich γ–γ′ BCs. In backscattering mode, the brighter phase represents γ′-Ni_3Al because of Pt enrichment and the darker phase represents γ-Ni. The 5/2 coatings were single-phase γ′-Ni_3Al below the oxide scale while the 5/5 coatings were γ′-Ni_3Al with a small volume fraction of $L1_0$ martensitic β phase because of the higher Al content in 5/5 BC. The thickness of the coatings, defined as the lower limit of the large inward growing Pt-rich γ′-Ni_3Al grains, was about 28 and 40 μm for 5/2 and 5/5 compositions respectively. From the TGO to the substrate, the microstructure of both γ–γ′ BCs evolved from Pt-rich single-phase γ′ to Pt-rich γ–γ′. After heat treatment, the average composition

Table 3 Tested TBC systems

SX	RE layer	BC	Cu	Name
Complete SPS TBC systems				
AM1	Hf	5/5	No	SPS AM1-5
			Yes	SPS AM1-5+Cu
		5/2	No	SPS AM1-2
			Yes	SPS AM1-2+Cu
N5			Yes	SPS N5-2+Cu
MCNG				SPS MCNG-2+Cu
TBC systems with an EBPVD thermal barrier				
AM1	Hf	5/5	No	EBPVD AM1-5
		5/2		EBPVD AM1-2
	No	β-(Ni,Pt)Al		Reference

SX single-crystal superalloy, *RE* reactive element, *BC* bond-coating

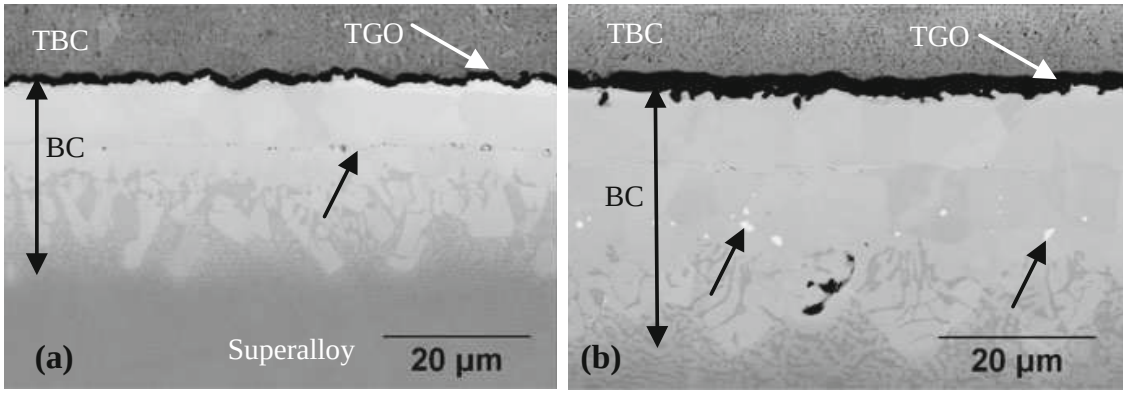

Fig. 1 SEM-BSE micrographs of two SPS systems after heat treatment: **a** AM1-2. The *black arrow* shows small cavities formed because of foil stacking. **b** AM1-5. The *two black arrows* exhibit few TCP phases. (*TBC* thermal barrier coating, *TGO* thermally grown oxide, *BC* bond-coating)

of the γ' layer under the TGO for all 5/2 BCs was typically 42Ni-21Al-22Pt-7Cr-3.5Co-1.2Ti-1.3Ta-1.5Mo-0.5W in at.%. For 5/5 BCs, EDS gave a typical composition, below the oxide scale, of 52Ni-21Al-13Pt-6Cr-4Co-1.4Ti-1.1Ta-1.0Mo-0.5W in at.%. Just below the TGO, the 5/5 BCs were even richer in Al, γ'-Ni_3Al being in equilibrium with a few precipitates of the martensitic β phase. These chemical analyzes confirmed the achievement of one Pt-rich and Al-rich BCs, but with slightly lower Pt than expected because of its diffusion toward the superalloy and lower Al due to its partial substitution by Ti and Ta. Nevertheless, the 5/5 BC presented a higher Al reservoir since it was thicker than the 5/2. The mean grain size of SPS AM1-2 BC was 6.3 ± 0.7 µm while that of the SPS AM1-5 BC was 10 ± 1.0 µm. After fabrication and heat treatment, it was checked by SEM and EPMA on similar systems that Cu was in solid solution in the phases of the BC. Cu doping did not affect the chemical compositions of major elements. For the samples used in this study, the detection limit of the EDS system did not allow Cu detection. By EDS, only Al_2O_3 could be detected within the oxide layer for all SPS systems. Previous work has shown that the alumina scale formed during the SPS process of TBC systems was α-Al_2O_3 [17]. The thickness of the TGO scale varied with BC composition. It was $\sim 1.7 \pm 0.3$ µm for SPS AM1-2 systems and 3.0 ± 0.5 µm for SPS AM1-5 systems because of the longer heat treatment of 5/5 BCs. No pegs were observed in any systems. However, small cavities in the outer zone of the coating at around 10 µm from the BC surface were observed for all systems, as illustrated in Fig. 1a by a black arrow for the SPS AM1-2 system. These cavities arose from the foils stacking in the SPS process. Figure 1b shows also small white precipitates for the SPS AM1-5 system. Analyzed by EDS, these particles were rich in W and Mo, hence referred to as TCP phases. They are indicated on the picture by black arrows. These TCP phases were only present in SPS TBC systems with a 5/5 BC after manufacturing. They were not observed after thermal cycling. It was probably due to the initial formation of a β-NiAl phase during the 5/5 processing, W and Mo tending to partition more in γ' than in β.

Thermal Cycling

Life Span

Figure 2 shows the spallation kinetics for SPS TBCs during thermal cycling. The dashed line corresponds to the lifetime limit defined as 25 % of spalled area. Reference systems had a mean lifetime estimated at about 700 cycles. The SPS AM1-2 system reached the lifetime criteria after 766 cycles at 1,100 °C while the SPS AM1-5 system reached it after 461 cycles. Figure 2 shows also that Cu addition decreased the lifetime of 5/2 and 5/5 systems of by 100 and 200 cycles, respectively. It was shown before that the Cu thin layer addition on the superalloy increased the initial interdiffusion kinetics between Pt and Ni during the heat treatment in SPS and then improved the homogeneity of the coating and decreased the fabrication time by SPS [13]. The present results show that the Cu doping level (thickness of the initial Cu film) needs to be optimized to keep its positive effect on fabrication without affecting the durability of the system.

Nevertheless, when comparing Pt-rich γ–γ′ and β-(Ni,Pt)Al, it should be noted that these BCs were not covered with the same ceramic top coat which led to different failure modes. For complete SPS TBC systems, spallation occurred mainly on the sample sides and then propagated towards the disc center, as shown in Fig. 3, whereas spalling could happen in any region of the EBPVD samples. This slow propagation of cracks initiated at the sample sides in SPS systems has already been described [11, 18]. It was attributed to crack initiation at cavities resulting from foil stacking or trapping of small YPSZ grains between Al and Pt foils or between foils and the substrate [12]. Then, the lifetime of systems with a Pt-rich γ–γ′ BC was artificially decreased relative to systems with a β-(Ni,Pt)Al BC. In order to solve this problem, the next set of samples was prepared with only EBPVD top coat for both SPS Pt-rich γ–γ′ and for APVS β-(Ni,Pt)Al BCs.

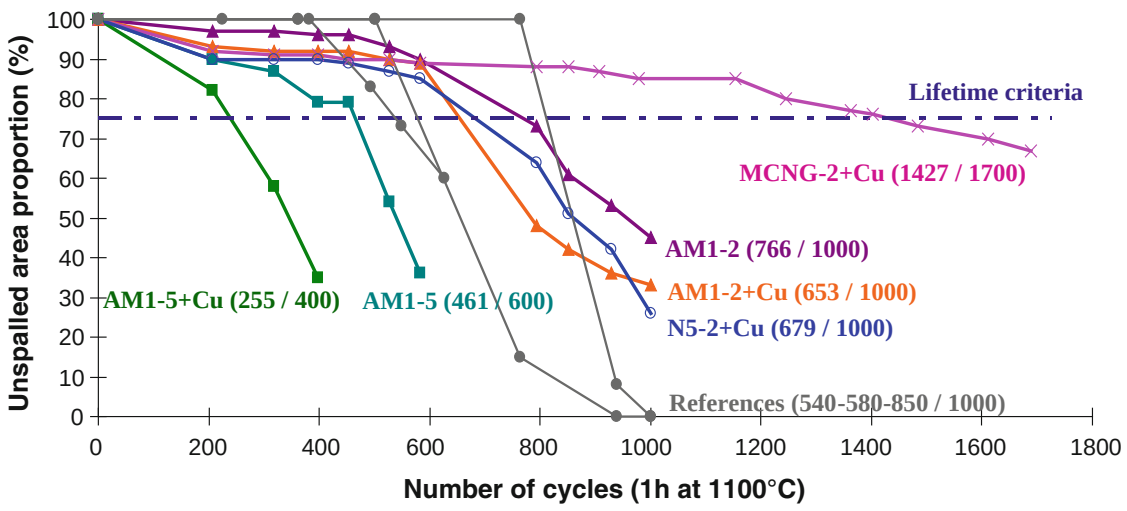

Fig. 2 Spalling kinetics during thermal cycling at 1,100 °C in air for SPS TBC systems. The *dashed line* represents the lifetime criteria. In *brackets* (lifetime/total number of cycles)

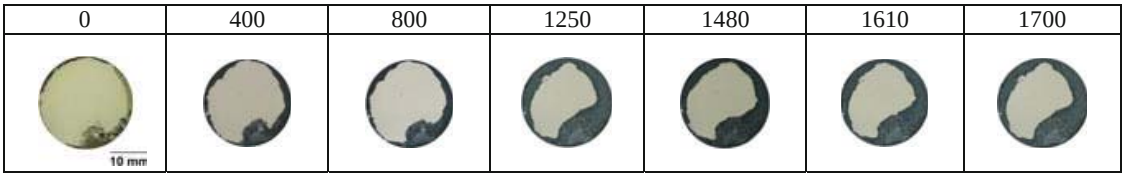

Fig. 3 Pictures of the SPS MCNG-2+Cu system versus the number of cycles at 1,100 °C

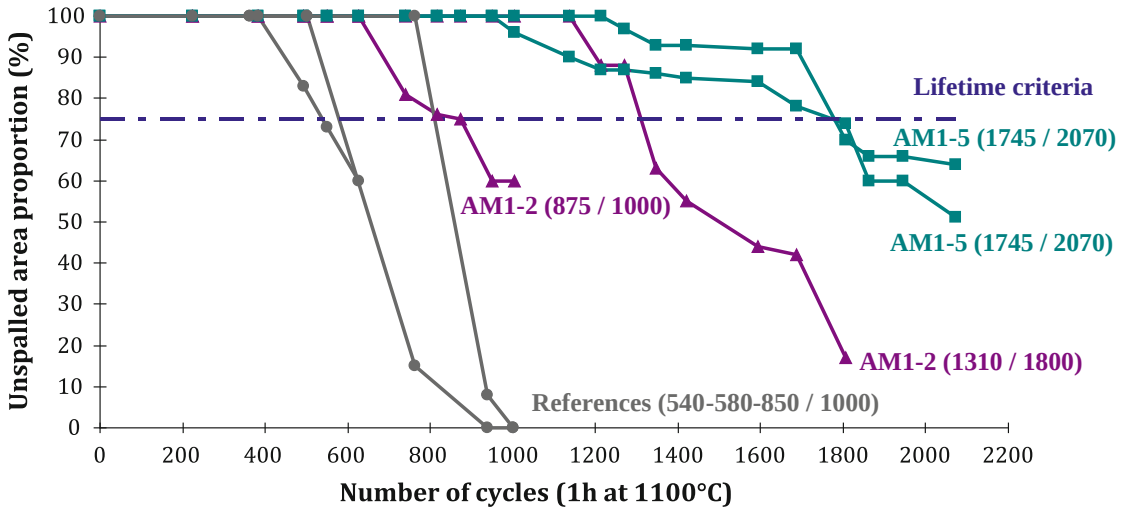

Fig. 4 Spallation kinetics during thermal cycling at 1,100 °C in air for EBPVD top coat systems. The *dashed line* represents the lifetime criteria. In *brackets* (lifetime/total number of cycles)

Figure 4 shows the spallation kinetics for systems with SPS Pt-rich γ–γ′ BCs and EBPVD top coats. All these systems showed a better thermal cycling resistance than the reference systems with an APVS β-(Ni,Pt)Al coating. The longest life span was obtained for EBPVD AM1-5 systems. Two samples were tested and both lasted 1,745 cycles. One did not exhibit any spallation before 1,200 cycles whereas the other started to spall after 1,000 cycles, mainly close to the edges. After 2,070 cycles, this same sample did not have any thermal barrier left because spallation had progressed from the edges towards the sample center. Concerning EBPVD AM1-2 systems, their life spans were 875 and 1,310 cycles. Although these results were not as good as those of the EBPVD AM1-5 systems, they were still better than the reference systems. It should be noted that this data revealed a longer lifetime for the 5/5 BC in the case of EBPVD top coats while longer lifetimes were obtained with the 5/2 BC for SPS TBC systems.

Microstructure After Thermal Cycling

SPS Systems SEM observations of cross sections were performed on all SPS TBC systems. Micrographs of an AM1-5 and AM1-2+Cu systems after 600 and 1,000 cycles, respectively at 1,100 °C are given in Fig. 5a, b. All the coatings underneath the TGO were fully Pt-rich γ–γ′ except the SPS AM1-5+Cu which was still single-phase Pt-rich γ′ after 400 cycles. The $L1_0$ martensitic β phase which had been observed after SPS for the AM1-5 systems disappeared. After 1,000 cycles, the BC

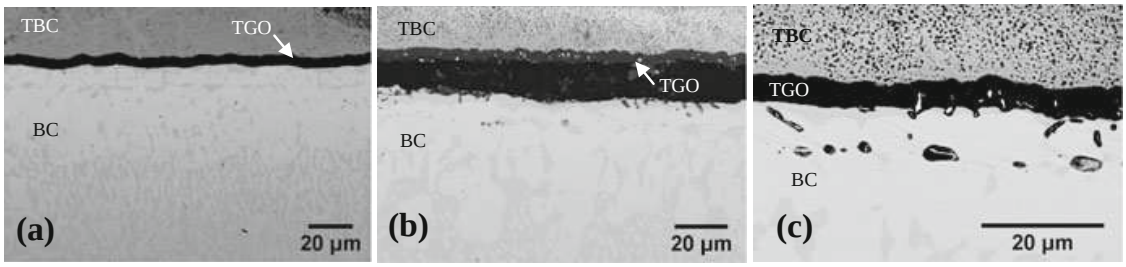

Fig. 5 SEM-BSE images of the cross-sections of SPS systems thermally cycled at 1,100 °C **a** AM1-5 system after 600 cycles **b** AM1-2+Cu system after 1,000 cycles **c** N5-2+Cu system after 1,000 cycles (*TBC* thermal barrier coating, *TGO* thermally grown oxide, *BC* bond-coating)

average thickness of the AM1-2 system was 50 µm and Pt had diffused up to 200 µm from the BC surface. The BC average thickness for the SPS AM1-5 system was similar to that of the SPS AM1-2 system (45 µm). In order to evaluate the possible remaining life span of the systems, the BC composition was analyzed by EDS underneath the TGO [5]. After 1,000 cycles at 1,100 °C, a BC composition of 60.5Ni-16Al-6.8Pt-4Cr-4Co-2.8Ti-3.7Ta-0.8Mo-1.4W in at.% was found for the SPS AM1-2 system. Similar concentrations were obtained for the SPS AM1-2+Cu system after 1,000 cycles. After 400 and 600 cycles, the average BC composition below the oxide scale of the SPS AM1-5 system was 58Ni-17.2Al-8Pt-5Cr-4.5Co-2.2Ti-2.9Ta-1.0Mo-1.2W in at.%. Cu was not detected by EDS after cycling but these analyzes indicate that Cu has no effect on long-term interdiffusion. They show also that Ti and Ta concentrations below the TGO were greater than those of the AM1 superalloy (Table 1). Such Ti and Ta enrichment had already been seen by Tawancy et al. [9, 19] in Pt-rich γ–γ' BCs and by Rouaix-Vande Put et al. [20] in Pt-modified NiCoCrAlYTa overlay coatings and could be due to a decrease of Ti and Ta activities in presence of Pt, as suggested in [21]. Similar effect has already been observed with Pt and Al [6].

TBCs failure occurred mainly at the BC/TGO interface. The same failure mode was observed by Pint et al. [10] for Pt-rich γ–γ' BCs fabricated by Pt electroplating and CVD process on second and third generation superalloys, after cycling at 1,150 °C. Rumpling and TCP phases were not observed in our samples. The TGO scale thickness did not vary much with the BC composition. It was about 4.1 ± 1.1 µm for all the SPS AM1 systems after 1,000 cycles at 1,100 °C. Only Al_2O_3 could be detected in the TGO for the SPS AM1-5 systems while Hf-rich oxides (white particles) were observed in the Al_2O_3 scale of the SPS AM1-2 and AM1-2+Cu systems. In this study, two rods of AM1 superalloy were used containing similar Hf, S and C levels. The thickness of the Hf layer deposited before BC manufacturing was kept constant between the systems. The presence of Hf-rich oxides in 5/2 systems can be due to the fact that initially a 5/2 BC was thinner than a 5/5 BC, hence the Hf concentration was higher in the AM1-2 system than in the AM1-5 system.

After processing, some SPS TBCs showed cracks at the depth where cavities resulting from the foil stacking were formed: one crack about 30 µm long was observed for the AM1-2 system. For the AM1-5 system, longer cracks up to 290 µm long were formed at the initial superalloy surface. The local poor foil adhesion after

cycling was a common damaging event for these SPS systems which led to void and crack formation during cycling and therefore to early failure.

Systems with EBPVD Top Coats Two AM1-5 systems and two AM1-2 systems with an EBPVD top coat were characterized by SEM. One of each system was observed after 230 cycles (Fig. 6a, b). The other systems were characterized after 2,070 cycles for EBPVD AM1-5 system and after 1,800 cycles for EBPVD AM1-2 system (Fig. 6c, d). After 230 cycles at 1,100 °C, both systems exhibited a BC with a Pt-rich γ–γ' microstructure. The BC thickness was around 50 µm for the AM1-5 system and 60 µm for the AM1-2 system (Fig. 6a, b). BC composition for both systems was measured by EDS underneath the surface. After 230 cycles, similar compositions were obtained for both systems and were on average 58Ni-15.1Al-8.1Pt-6.2Cr-4.9Co-2.0Ti-3.0Ta-1.2Mo-1.5W in at.%. Al and Pt concentrations obtained for the EBPVD systems after 230 cycles were close to those obtained for the SPS AM1-2 system but after 1,000 cycles (16Al-7Pt in at.%). The fact that the Pt level underneath the TGO seems to decrease faster for the system with the EBPVD top coat than with the SPS top coat may be due to the difference in the fabrication process. Indeed, in the EBPVD process, there is an additional alumina grit-blasting step after the SPS processing of the BC. This grit-blasting step may introduce dislocations in the coating, acting as a diffusion short circuit. Alternatively, the grit-blasting may remove brittle parts of the coating before EBPVD, therefore decreasing the Pt quantity.

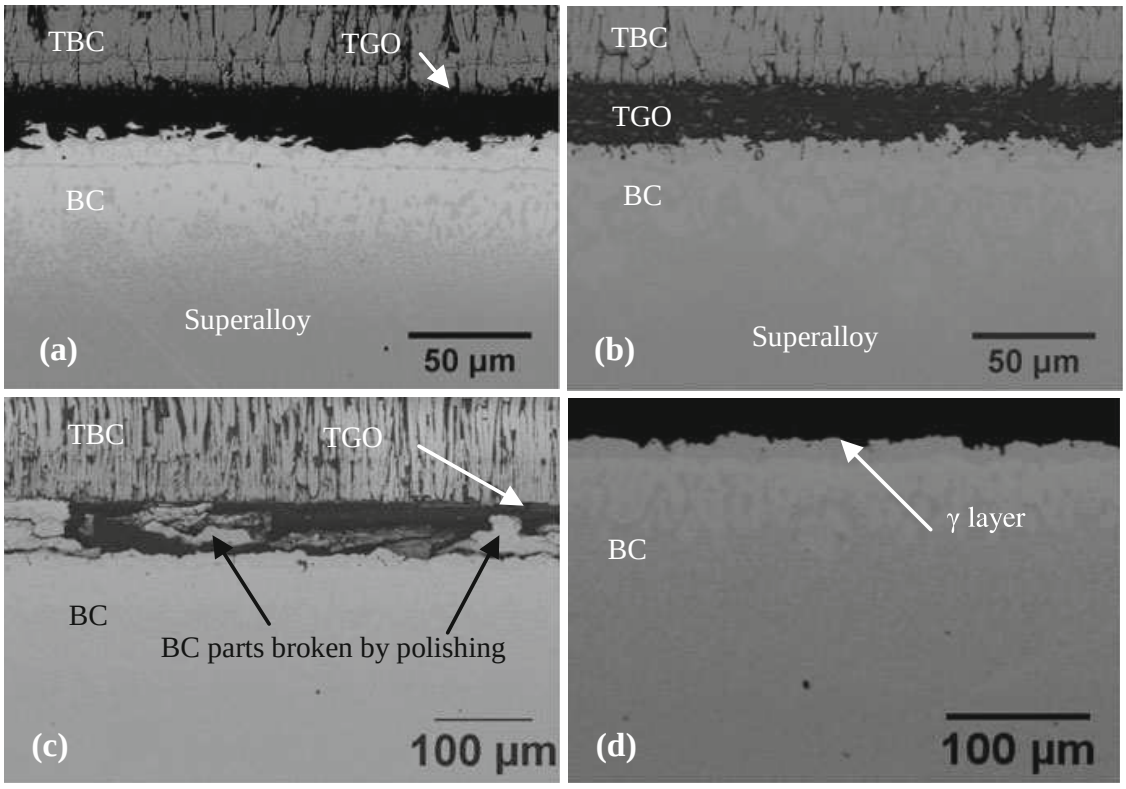

Fig. 6 Cross-section images of TBC systems with an EBPVD top coat after thermal cycling at 1,100 °C **a** AM1-5 after 230 cycles **b** AM1-2 after 230 cycles **c** AM1-5 after 2,070 cycles **d** AM1-2 after 1,800 cycles. (*TBC* thermal barrier coating, *TGO* thermally grown oxide, *BC* bond-coating)

In addition, in both cases, the oxide scale was damaged and the failure occurred at the BC/TGO interface (Fig. 6b). No rumpling appeared after 230 cycles but the presence of many pegs for the EBPVD AM1-2 system generated a non linear BC surface. The selective Al oxidation led to the formation of a thin continuous γ layer after only 230 cycles, Fig. 6b. No TCP phases formed during the thermal cycling. The Pt-rich γ–γ′ microstructure was still observed for both systems after a longer thermal cycling, that was 2,070 cycles for EBPVD AM1-5 system and 1,800 cycles for EBPVD AM1-2 system (Fig. 6c, d). The BC thickness was around 60 μm for EBPVD AM1-5 and 70 μm for EBPVD AM1-2. The γ layer already formed underneath the TGO after 230 cycles was now thicker. Its average composition was 60.1Ni-5.8Al-3.3Pt-15.4Cr-7.9Co-1.2Ti-1.9Ta-2.4W-2.0Mo in at.%.

Although the oxide scale in TBC systems with an EBPVD top coat was damaged after only 230 cycles (Fig. 6b) those systems showed a better thermal cycling resistance than full-SPS systems. The TGO damage could be due to metallographic preparation issues since these systems seemed to be brittle, as seen on the BC parts broken by the polishing (Fig. 6c). The life span results obtained for EBPVD systems must be moderated compared with SPS system lifetimes. Indeed, when using SPS to produce TBC systems, some fabrication issues appeared mainly on the sample sides. If the disc edges were perfectly covered like for EBPVD samples, the spallation may not have occurred promptly and progressed so rapidly.

All TBC systems tested in this study were fabricated with 5 μm of Pt. Despite the fabrication defects observed within the SPS BCs, most systems have shown better thermal cycling resistance than reference TBC systems which were fabricated with a thicker Pt layer. This shows the intrinsic superiority of Pt-rich γ–γ′ BC doped in Hf over β BC even with a lower Pt addition.

Substrate Effect

Two SPS TBC systems with a 5/2+Cu BC composition on different superalloys (N5 and MCNG) were also thermally cycled at 1,100 °C to evaluate the substrate effect on the TBC lifetime (Fig. 2). The SPS MCNG-2+Cu system showed a much better cyclic oxidation resistance than AM1-2+Cu and N5-2+Cu systems. The MCNG system lifetime was estimated at 1,430 cycles and was further doubled when compared to the other SPS systems. Figure 5c shows that the SPS N5-2+Cu system still exhibited a two phase Pt-rich γ–γ′ BC after 1,000 cycles. Its BC thickness was nearly the same as that of the AM1-base system (∼50 μm) but the extent of Pt diffusion was smaller. The BC composition below the oxide scale for the SPS N5-2+Cu system was still Al-rich (18 at.%) but depleted in Pt (5 at.%) after 1,000 cycles. Concerning the TGO, it was composed of Al_2O_3 and many Hf-rich oxide precipitates. These pegs were also seen for the AM1 and MCNG systems, but in lower quantities. Voids created during SPS processing were still present at the same depth (7–8 μm thick) as originally but they extended.

The higher oxidation resistance, under thermal cycling conditions at 1,100 °C, of MCNG-base systems when compared to AM1-base system had already been observed with a β-(Ni,Pt)Al BC [22] and also when compared to AM3-based system with a Pt-modified MCrAlY overlay coating [20]. This better resistance can be

interpreted by the positive effect of Hf present in the superalloy. This beneficial effect has already been observed in the cyclic oxidation of aluminide BCs [23]. The Co level can also explain this better resistance. Indeed, Wu et al. [10, 24] recently demonstrated that a higher Co content in the superalloy may be detrimental to Pt diffusion coating performance. As MCNG is a Co-free superalloy, the large endurance of the MCNG-2+Cu system could be attributed to the absence of Co. In addition, it appeared that the N5-2+Cu system lasted as long as the AM1-2+Cu one, around 700 cycles. Knowing that Ti has a detrimental effect on the thermal cycling resistance [9, 25] and that René N5 is a Ti-free superalloy, this result is surprising. However, it should be noted that René N5 superalloy contained higher Co and Hf contents than AM1. As many Hf-rich oxides formed in this system, the BC might be overdoped in Hf, decreasing its lifetime. Also, as only one sample of N5-base system was cycled, this result needs to be confirmed by testing more samples.

Conclusions

With a view to develop new BC compositions for advanced TBC systems, various TBC systems with Pt-rich γ–γ′ BCs were tested via cyclic oxidation at 1,100 °C. Two main BC compositions were fabricated by SPS, one was Pt-rich and the other was Al-rich, in order to compare their thermal cycling resistance to that of the standard β-(Ni,Pt)Al diffusion BC. The addition of Cu and Hf was also studied. The following conclusions can be drawn from this work. Most TBC systems comprising Pt-rich γ–γ′ BC showed a better thermal cycling resistance than the reference TBC systems [β-(Ni,Pt)Al APVS+YPSZ EBPVD] despite the fabrication defects observed within the SPS BCs. This confirms the intrinsic superiority of Pt-rich γ–γ′ BCs doped in Hf over β-(Ni,Pt)Al BCs even with a smaller Pt addition. For TBC systems with a SPS-processed BC and top coat, 5/2 systems (Pt-rich) were more resistant to spallation than 5/5 systems with a lifetime estimated at more than 750 cycles. For TBC systems with a SPS-processed BC and an EBPVD top coat, a better oxidation behavior was obtained for the 5/5 systems (Al-rich) which can resist large spallation up to 1,700 cycles. For both systems (SPS and EBPVD), the failure occurred at the BC/TGO interface. A continuous γ layer had formed during thermal cycling beneath the TGO because of Al depletion. This layer was enriched in Cr and Co and depleted in Al and Pt. This likely explains the loss of scale adherence of these systems. Further chemical investigations are needed to link TGO adherence with the precise chemical composition of the γ layer. Although Cu played a positive role in the SPS processing, this element had a negative effect on the system life span. Therefore, the Cu level needs to be optimized. The comparison of oxidation performance between 5/2+Cu SPS TBC systems deposited on three different superalloys revealed that the MCNG-base system had the best cyclic oxidation behavior since it lasted 1,430 cycles whereas AM1 and René N5-base systems exhibited 25 % of spalled area after 680 cycles.

Acknowledgments A part of this study was performed with the financial support of DGA and SNECMA. Superalloys were furnished by Snecma-SAFRAN Company. RF-sputtering was done at ICMCB, Bordeaux, France and EBPVD deposits at Ceramic Coating Center, Châtellerault, France.

References

1. T. Izumi, N. Mu, L. Zhang and B. Gleeson, *Surface and Coatings Technology* **202**, (4–7), 628 (2007).
2. N. Mu, T. Izumi, L. Zhang and B. Gleeson, *Materials Science Forum* **595–598**, 239 (2008).
3. J. L. Smialek and R. F. Hehemann, *Metallurgical Transactions* **4**, (6), 1571 (1973).
4. R. T. Wu, X. Wang and A. Atkinson, *Acta Materialia* **58**, (17), 5578 (2010).
5. S. Selezneff, M. Boidot, J. Hugot, D. Oquab, C. Estournès and D. Monceau, *Surface and Coatings Technology* **206**, 1558 (2011).
6. B. Gleeson, W. Wang, S. Hayashi and D. Sordelet, *Materials Science Forum* **461–464**, 213 (2004).
7. J. A. Haynes, B. A. Pint, Y. Zhang and I. G. Wright, *Surface and Coatings Technology* **202**, 730 (2007).
8. R. T. Wu, K. Kawagishi, H. Harada and R. C. Reed, *Acta Materialia* **56**, 3622 (2008).
9. H. M. Tawancy, A. I. Mohamed, N. M. Abbas, R. E. Jones and D. S. Rickerby, *Journal of Materials Science* **38**, 3797 (2003).
10. B. A. Pint, J. A. Haynes and Y. Zhang, *Surface and Coatings Technology* **205**, (5), 1236 (2010).
11. D. Monceau, D. Oquab, C. Estournes, M. Boidot, S. Selezneff, Y. Thebault and Y. Cadoret, *Surface and Coatings Technology* **204**, (6–7), 771 (2009).
12. M. Boidot, Elaboration de revêtements γ–γ' et de systèmes barrière thermique par Spark Plasma Sintering, PhD Thesis, Institut National Polytechnique de Toulouse (2010).
13. S. Selezneff, Etude et développement de revêtements γ–γ' riches en platine, élaborés par Spark Plasma Sintering (SPS). Application au système barrière thermique, PhD Thesis, Institut National Polytechnique de Toulouse (2011).
14. S. Hayashi, S. I. Ford, D. J. Young, D. J. Sordelet, M. F. Besser and B. Gleeson, *Acta Materialia* **53**, (11), 3319 (2005).
15. C. C. Jia, K. Ishida and T. Nishizawa, *Metallurgical and Materials Transactions A* **25**, (3), 173 (1994).
16. J.-Y. Guédou, M. Boidot, C. Estournès, D. Monceau, D. Oquab, and S. Selezneff, FR Patent No 11 53 678, (29th April 2011).
17. M. Boidot, S. Selezneff, D. Monceau, D. Oquab and C. Estournès, *Surface and Coatings Technology* **205**, (5), 1245 (2010).
18. D. Monceau, D. Oquab, C. Estournes, M. Boidot, S. Selezneff and N. Ratel-Ramond, *Materials Science Forum* **654–656**, 1826 (2010).
19. H. Tawancy and L. M. Al-Hadhrami, *Journal of Engineering for Gas Turbines and Power* **133**, 042101 (2011).
20. A. Rouaix-Vande Put, D. Oquab, A. Raffaitin, and D. Monceau, *Corrosion Science*, (Submitted in 2012).
21. A. Vande Put, D. Oquab and D. Monceau, *Materials Science Forum* **595–598**, 213 (2008).
22. C. Duhamel, M. Chieux, R. Molins, L. Rémy, D. Monceau, A. Vande Put and J.-Y. Guedou, *Materials at High Temperatures* **29**, (2), 136 (2012).
23. I. J. Bennett and W. G. Sloof, *Materials and Corrosion* **57**, (3), 223 (2006).
24. R. T. Wu and R. C. Reed, *Acta Materialia* **56**, (3), 313 (2008).
25. N. Vialas and D. Monceau, *Oxidation of Metals* **66**, (3–4), 155 (2006).